Atmos. Meas. Tech. Discuss., 6, 10443–10480, 2013
www.atmos-meas-tech-discuss.net/6/10443/2013/
doi:10.5194/amtd-6-10443-2013

Atmospheric Measurement Techniques Discussions
Open Access

Mobile air monitoring data processing strategies and effects on spatial air pollution trends

H. L. Brantley[1,2], **G. S. W. Hagler**[1], **S. Kimbrough**[1], **R. W. Williams**[3], **S. Mukerjee**[3], **and L. M. Neas**[4]

[1]US Environmental Protection Agency, Office of Research and Development, National Risk Management Research Laboratory, Research Triangle Park, North Carolina, USA
[2]Student Services Contractor, Research Triangle Park, North Carolina, USA
[3]US Environmental Protection Agency, Office of Research and Development, National Exposure Research Laboratory, Research Triangle Park, North Carolina, USA
[4]US Environmental Protection Agency, Office of Research and Development, National Health and Environmental Effects Research Laboratory, Chapel Hill, North Carolina, USA

Received: 1 November 2013 – Accepted: 25 November 2013 – Published: 5 December 2013

Correspondence to: G. S. W. Hagler (hagler.gayle@epa.gov)

Published by Copernicus Publications on behalf of the European Geosciences Union.

Abstract

The collection of real-time air quality measurements while in motion (i.e., mobile monitoring) is currently conducted worldwide to evaluate in situ emissions, local air quality trends, and air pollutant exposure. This measurement strategy pushes the limits of traditional data analysis with complex second-by-second multipollutant data varying as a function of time and location. Data reduction and filtering techniques are often applied to deduce trends, such as pollutant spatial gradients downwind of a highway. However, rarely do mobile monitoring studies report the sensitivity of their results to the chosen data processing approaches. The study being reported here utilized a large mobile monitoring dataset collected on a roadway network in central North Carolina to explore common data processing strategies including time-alignment, short-term emissions event detection, background estimation, and averaging techniques. One-second time resolution measurements of ultrafine particles ≤ 100 nm in diameter (UFPs), black carbon (BC), particulate matter (PM), carbon monoxide (CO), carbon dioxide (CO_2), and nitrogen dioxide (NO_2) were collected on twelve unique driving routes that were repeatedly sampled. Analyses demonstrate that the multiple emissions event detection strategies reported produce generally similar results and that utilizing a median (as opposed to a mean) as a summary statistic may be sufficient to avoid bias in near-source spatial trends. Background levels of the pollutants are shown to vary with time, and the estimated contributions of the background to the mean pollutant concentrations were: BC (6 %), $PM_{2.5-10}$ (12 %), UFPs (19 %), CO (38 %), PM_{10} (45 %), NO_2 (51 %), $PM_{2.5}$ (56 %), and CO_2 (86 %). Lastly, while temporal smoothing (e.g., 5 s averages) results in weak pair-wise correlation and the blurring of spatial trends, spatial averaging (e.g., 10 m) is demonstrated to increase correlation and refine spatial trends.

AMTD
6, 10443–10480, 2013

1 Introduction

Air quality research has been revolutionized in recent years by the development and application of mobile platforms capable of resolving air pollutant concentrations in real time. These platforms – including instrumented cars, vans, bicycles, and handheld devices – have been enabled by advancements in air monitoring instrumentation, such as higher time resolution and greater portability, as well as improvements in location resolution using commercially available global positioning systems (GPSs). The mobile measurement strategy has been utilized for a diversity of applications, which can be loosely categorized as: (1) emissions characterization, (2) near-source assessment, and (3) general air quality surveying (Table 1).

Mobile monitoring is often chosen over other methods for its ability to efficiently obtain data at a high spatial resolution under a variety of different conditions. Emissions estimation can be conducted using a number of methods, including chassis dynamometer experiments, tunnel studies, and remote sensing, but mobile monitoring methods are often selected because they enable researchers to obtain in-use emissions estimates of individual vehicles under a variety of operating conditions (Park et al., 2011; Wang et al., 2009, 2011, 2012; Westerdahl et al., 2009).

In near-source environments, pollutant concentrations can vary on the scale of tens of meters. To characterize this spatial variation, dense networks of stationary monitors can be deployed, but mobile monitoring is often preferred because of the increased spatial flexibility (Baldauf et al., 2008; Choi et al., 2012; Durant et al., 2010; Hagler et al., 2012; Kozawa et al., 2009; Zwack et al., 2011a; Rooney et al., 2012; Westerdahl et al., 2005; Drewnick et al., 2012; Massoli et al., 2012). Broader surveys of ambient air quality are also frequently conducted using mobile monitoring on a scale ranging from neighborhood to country to characterize regional concentrations or locate previously unknown hotspots (Hagler et al., 2012, 2010; Arku et al., 2008; Adams et al., 2012; Farrell et al., 2013; Drewnick et al., 2012; Van Poppel et al., 2013; Hu et al., 2012).

AMTD
6, 10443–10480, 2013

A myriad of post-processing strategies have been applied to mobile monitoring data to answer specific research questions including algorithms fine-tuning temporal alignment, temporal or spatial smoothing, local background estimation, and detection of short-term emissions events (Table 1). Precise alignment of instruments with location data is universally important for mobile monitoring conducted while moving at relatively high speeds. If the vehicle is traveling at merely 10 m s^{-1} (22 mph), a two-second misalignment between an instrument and the GPS-derived location can introduce approximately 20 m of error.

After optimal alignment, extracting meaningful information from mobile monitoring data and developing intuitive visuals often requires further processing steps. For example, ultrafine particle data collected while driving on a roadway network would represent the temporal variation in local emissions and urban background, with spatial variation expected as the monitoring platform moves along a route, and evidence of short-term concentration spikes due to occasional emissions in very close proximity. Depending on the research question, different data processing steps may be applied to separate the component of interest from the other causes of variation (Fig. 1). If a researcher is interested in general spatial variation attributed to local sources, it may be desirable to minimize the influence of background variation and short-term concentration spikes caused by nearby exhaust events.

A variety of algorithms for emissions event detection and background standardization have been employed and published in the past several years (Table 2). Event detection is important both for studies that seek to estimate emission factors but also to minimize the impact of sporadic proximate exhaust when determining near-source spatial trends. Background estimation is important for extracting local-scale influences from regional background, and standardization of background is important for general air quality surveying studies which may have unique sampling routes measured over different days. Regional influences such as meteorology can cause background concentrations to vary both diurnally and daily. Without background standardization, the variable background may be erroneously attributed to spatial variation. Background

AMTD
6, 10443–10480, 2013

standardization becomes particularly important for pollutants with high background relative to the total concentration. One method of background standardization is to keep the length of the sampling run short enough that temporal variation due to regional influences can be assumed to be minimal. Another approach is to complete several laps of the same route on each sampling day (e.g., Van Poppel et al., 2013), ensuring that each location measured along the route has the same representation of average background over the multiple sampling days. However, when a route completion exceeds the timeframe within which the regional background changes or comparisons are being made of multiple routes measured on different days, temporal variation of the background is an important consideration.

As a final data processing step, temporal or spatial smoothing is often applied either to reduce noise in the data or more effectively display trends (Westerdahl et al., 2005; Weijers et al., 2004; Pirjola et al., 2012). Applying a rolling median or mean can be used to maintain the high temporal resolution while reducing the amount of noise and influence of extreme outliers. Aggregating the data to a longer time window can also be used to reduce the influence of noise or to reduce the degree of autocorrelation among the measurements. Types of spatial smoothing include calculating median or mean values along fixed length intervals of the route or within a fixed radius of locations of interest.

Recently, efforts have been made to study the mobile monitoring approach. For example, Van Poppel et al. (2013) evaluated how many sampling route repeats were required to develop a representative data set. However, a rigorous examination of mobile monitoring data processing steps and the implications for the derived results is needed. This study utilizes a robust multipollutant mobile monitoring data set collected on a roadway network in North Carolina, USA to evaluate common data-processing methods, including time alignment optimization, emissions event detection, background standardization, and spatial and temporal smoothing.

AMTD
6, 10443–10480, 2013

2 Methods

2.1 Experimental data

An intensive mobile monitoring campaign was conducted in the Research Triangle Area of North Carolina in the summer of 2012 as part of the Research Triangle Area Mobile Source Emission Study (RAMSES). Measurements were collected using a converted all-electric PT Cruiser, described in Hagler et al. (2010). Six instruments were securely installed on board the vehicle: an engine exhaust particle sizer (EEPS) (Model 3090, TSI, Shoreview, MN, USA) which provided size-resolved ultrafine and accumulation mode particle counts, an aerodynamic particle sizer (APS) (Model 3321, TSI, Shoreview, MN, USA) for size-resolved particle counts in fine to coarse mode, a portable aethalometer (AE42, Magee Scientific, Berkeley, CA, USA) that measured black carbon (BC), a dual quantum cascade laser (QCL) (Aerodyne Research, Inc., Billerica, MA, USA) that measured carbon monoxide (CO), a non-dispersive infrared (NDIR) gas analyzer that measured carbon dioxide (CO_2) (Li-COR 820, LiCOR Biosciences, Lincoln, NE, USA), and a cavity attenuated phase shift (CAPS) monitor that measured nitrogen dioxide (NO_2) (Aerodyne Research, Inc., Billerica, MA, USA). All instruments used had a sampling rate of one second.

The campaign included 12 routes within Wake, Durham, and Orange counties, North Carolina. The routes covered areas that had previously been classified using modeled traffic data as areas of traffic delay, high traffic volume, transit routes, high signal light density, and urban area. Mobile monitoring was conducted during morning rush hour (07:00–10:30 a.m. LT) on 24 weekdays between 23 August and 11 October 2012, with each run consisting of three or more laps and each route covered on two sampling days. The routes ranged from 5.2–18.1 km in length.

AMTD
6, 10443–10480, 2013

2.2 Data processing methods

Mobile monitoring data were processed and displayed using MATLAB (2012), ArcGIS (ESRI, 2011) and R version 2.15.1 (R Core Team, 2012) along with the R packages scatterplot3d (Ligges and Mächler, 2003), openair (Carslaw and Ropkins, 2012), and mcgv (Wood, 2003). A noise-reduction algorithm was applied to black carbon concentrations to reduce the frequency of negative values (Hagler et al., 2011). Examples of emissions quantification, near-source air quality gradients, and general air quality surveying were selected to illustrate the implications of the following data processing steps: fine-tuning time alignment of multipollutant data, background standardization, emissions event detection, spatial smoothing and temporal smoothing.

Two methods of time alignment were compared: the engineering process and the cross-correlation method (Choi et al., 2012). The engineering process typically used in mobile monitoring campaigns consists of applying a concentration change (high efficiency particulate air filter for particle instruments, gas standard for gas instruments) at the inlet and noting the instrument response time. The cross-correlation method can be used as a fine-tuning step when multiple pollutants produced by a single source are measured and involves calculating the correlation coefficient between two co-emitted pollutants at various time lags. Because the pollutants are co-emitted, the best estimate of the difference in response times between the instruments can be assumed to correspond with the lag time that produces the maximum correlation coefficient (Choi et al., 2012). As an illustration of the impact precise time alignment can have on analysis results, emissions factors were calculated using the method described by Park et al. (2011) for a single emissions event identified using the test vehicle's webcam footage (Fig. 2). Fuel-based emissions factors for BC, CO, and ultrafine particles (diameter $\leq$ 100 nm, UFPs) were expressed in terms of pollutant mass or particle number emitted per kilogram of fuel burned by normalizing the integrated change in pollutant concentration to total carbon concentration change. Volatile organic compounds (VOCs) were not measured, but for the purpose of this illustration the fraction of carbon

AMTD
6, 10443–10480, 2013

converted to VOCs during combustion was assumed to be negligible compared to the proportion emitted as CO_2. The emissions factors (EF_p) were calculated using the following equation:

$$EF_p = \frac{\Delta[P]}{(\Delta[CO_2] + \Delta[CO])} \cdot 0.85 \quad (1)$$

Where $\Delta[P]$ is the integrated change in pollutant concentration above roadway concentrations for the duration of the plume capture. Similarly, $\Delta[CO_2]$ and $\Delta[CO]$ are the integrated changes in the respective CO_2 and CO concentrations above the roadway concentrations. The target vehicle, identified on the monitoring vehicle's webcam and used to establish the aforementioned emission factor, was a light-duty gasoline vehicle, so 0.85 was used as the carbon weight fraction (Park et al., 2011). The roadway concentrations were calculated by fitting a straight line from the last measurement before the emissions event to the first measurement after the emissions event (Fig. 2). The roadway concentrations were subtracted from the measured concentrations, and the integrated change was calculated using a spline function in combination with integration to calculate a numerical integral. Emissions factors were calculated for both the 1 s measurements and 10 s averages (discrete windows), as well as with and without adjusting the temporal alignment using the cross-correlation method.

Three emissions event removal methods were compared: the running coefficient of variation (COV) method used by Hagler et al. (2012), the standard deviation of the background method used by Drewnick et al. (2012), and the rolling 25th percentile method used by Choi et al. (2012). Measurements of local exhaust tend to be both higher and more variable than measurements of well-mixed air. Both the COV method and the standard deviation of the background method rely on the high variability as well as the magnitude of measurements of local exhaust while the rolling 25th percentile relies solely on the magnitude. The running COV method (Hagler et al., 2012) was developed using UFP concentrations and consists of calculating the rolling 5 s standard deviation (2 s before and after the center data point) and dividing it by the

AMTD
6, 10443–10480, 2013

mean concentration of the sampling run. The 99th percentile of the calculated COV is used as a threshold (in Hagler et al., 2012, the threshold COV for UFPs was 2) and any data points with a COV above this threshold are flagged for removal along with the data points 2 s before and after. In the standard deviation of the background method, the standard deviation of measurements (UFP or CO_2) below the median is calculated (σ_b). Any measurement more than $3\sigma_b$ greater than the previous measurement is flagged. Subsequently, all measurements with concentration C_i that meets the following criteria are flagged:

$$C_i > C_{uf} + 3\sigma_b + \sqrt{n} \times \sigma_b \quad (2)$$

Where C_{uf} is the concentration of the last unflagged measurement and n is the number of measurements between C_{uf} and C_i. The rolling 25th percentile method involves calculating the 25th percentile of various time windows. Choi et al. (2012) used 53 s (26 s before and after the center data point) when the distance from a freeway was farther than 1 km, 31 s (15 s before and after) for distances between 300 m and 1 km, and 3 s (1 s before and after) within 300 m of a freeway. Because the majority of the data used in this comparison was between 300 m and 1 km, a 31 s window was used for the entire dataset to simplify the calculation. One final method of reducing the effect of local emissions is to use outlier resistant statistics such as the median instead of the mean.

A single run conducted on 11 October 2012, was chosen to compare these methods because of the large number of laps conducted (11) and favorable wind conditions (from the highway towards the transect). The route included a section of highway (AADT 109 000), a transect running at an angle to the highway with moderate traffic (AADT 32 000) and a low traffic road. As an illustration, gradients of CO, UFP, BC, and NO_2 along the highway transect were used to compare the effect of the emissions event removal methods on the 50 m mean concentrations and with the 50 m median concentration of the unfiltered data.

AMTD
6, 10443–10480, 2013

A new method of estimating the time-varying contribution of the regional background was developed and compared with the use of a low percentile (Bukowiecki et al., 2002). This method could not be compared with averaging measurements by fixed monitoring sites (Arku et al., 2008) or designating a background area (Hagler et al., 2012; Van Poppel et al., 2013) because no stationary monitoring was conducted concurrently with the mobile monitoring and the same background zone was not covered on each sampling run. Zwack et al. (2011a, b) also used a time-varying background estimation, but instead of estimating background concentrations separately, a smooth function of time over each sampling run was included as a term in the linear regression used to determine concentration differences.

Ultimately, the results of spatial and temporal smoothing were compared. The average speed of the monitoring vehicle on the route used to compare temporal and spatial smoothing was approximately 10 m s^{-1}. The smoothing intervals chosen for comparison were a 5 s and 10 s window, and 10 m, 50 m, and 100 m segments. The same route chosen to compare emissions event detection was used to compare smoothing methods. For this comparison, data from sampling runs conducted on 11 October 2012 and 21 September 2012 were used and Spearman correlation coefficients were calculated for CO, BC, UFPs, NO_2, $PM_{2.5}$ and CO_2.

3 Results and discussion

The results described in this paper focus on the data from a few of the routes and the implications of various data processing steps. The complexity of the pre-processing and analysis of mobile monitoring data precludes a detailed assessment of all study results in this paper.

AMTD
6, 10443–10480, 2013

3.1 Data alignment

For the current instrument setup, the time between a concentration change at the inlet and visual inspection of instrument response ranged from 0 s to 5 s for both real-time gas and particle instruments (Fig. 3). Using the engineering method, the response time of the QCL (CO) and APS (particle count in fine to coarse range) was less than 1 s, the CAPS (NO_2) and aethalometer (BC) was 4 s, and the Li-COR (CO_2) and EEPS (UFP) was 5 s.

After applying the lags determined using the engineering method, the cross-correlation method was used to fine-tune the alignment. CO was chosen as the reference measurement because the quantum cascade laser was the most sensitive instrument with the fastest response time. Because the primary source of CO and BC in the study area was vehicle exhaust, it was assumed that the maximum correlation would occur when the measurements were perfectly aligned. Using the cross correlation method, the measured BC concentration was found to lag the CO concentration by 3 s (Fig. 4). The other particle instruments were also found to lag the CO measurement by 3 s. The CO_2 measurement was found to lead the CO measurement by 4 s. The only pollutant measured that was not strongly correlated with CO at a specific lag time was NO_2; however, NO_2 was strongly correlated with UFPs at a lag of 0 s, so the lag used for UFPs (3 s) was also applied to NO_2.

Emissions factors for a specific vehicle and specific driving condition were calculated for CO, UFPs, and BC using the data aligned by the engineering tests and the data with the lag times adjusted to maximize correlations. A 10 s average was also calculated to compare the effect of the time-base on the emissions factor calculation and temporal alignment. Using 10 s measurements resulted in higher estimates of emissions and greater differences between the data adjusted using the cross-correlation method and the un-adjusted data (Table 3). Using the 1 s data, the alignment adjustment changed the emissions factors by 0.5 %, 7 %, and 25 % for UFPs, CO, and BC respectively; while for the 10 s data alignment adjustment changed the emissions factors by 26 %,

AMTD
6, 10443–10480, 2013

12 %, and 61 %, respectively. In this example, the correct values are not known, but this illustration demonstrates the relative effect of a shift in alignment by a few seconds on the resulting emissions factors.

3.2 Comparison of methods of filtering emissions events

Three emissions event filtering methods and their effect on the shape of the pollutant gradient were compared using the data collected on 11 October 2012: the running COV method used by Hagler et al. (2012), the standard deviation of the background method used by Drewnick et al. (2012), and the rolling 25th percentile used by Choi et al. (2012). Using the COV method, several emissions events were identified on the transect over the course of the run (Fig. 5).

For near-source air monitoring studies, a common analysis is to consider concentrations as a function of distance from the source of interest (e.g., edge of road) (Karner et al., 2010). Similar to previous studies, elevated concentrations of mobile source pollutants were observed on the highway (boxplots in Fig. 6), and measured concentrations decreased with increased distance from the highway (Fig. 6). However, the mean 50 m concentrations along the transect are clearly affected by emissions events, as is evidenced by the mean concentrations of UFP, BC, NO_2 and CO at 250 m (Fig. 6). Using any of the emissions event filters or the median values substantially reduces the influence of these events. The 25th percentile filter results in the lowest estimates of concentrations along the transect because it affects all of the measurements, not just those influenced by local exhaust. The 25th percentile filter also results in the smoothest estimate of the gradient along the transect (Fig. 6).

Another important consideration is that different exhaust plumes contain different pollutant mixtures. For example, the plume that was encountered at 250 m caused spikes in all four exhaust indicators, while the plume encountered at 800 m caused increases in CO and UFPs but not in BC or NO_2 (Fig. 6). The measurements used as indicators of local exhaust must be chosen carefully to adequately remove the spikes

AMTD
6, 10443–10480, 2013

while retaining the majority of the data. For this run, by using both CO and UFP as indicators, the spikes in NO_2 and BC were successfully removed.

3.3 Comparison of background standardization methods

One method of accounting for background variation is to calculate a single value for each sampling run to use to normalize the concentrations. This value can be a fixed concentration such as the 1st or 10th percentile of the measurements (Bukowiecki et al., 2002) or can be added into a model as a random effect. However, in the present study over the course of a two hour sampling period, the baseline of the CO time series decreased from 400 ppb to 200 ppb (Fig. 7). Depending on the research question and the pollutant of interest, using a single value to normalize the data may introduce unnecessary error. A rolling minimum did not appear to be a good alternative. A 60 s rolling minimum is a better descriptor of variation in local concentrations than variation in urban background (Fig. 7b). A 300 s rolling minimum results in a more drastic stair-step pattern which is not descriptive of the change in background over time which generally changes very gradually.

In many studies, the sampling routes include a designated area that is considered background (Hagler et al., 2012; Van Poppel et al., 2013). The measurements made in this area over time can be separated out and used to normalize the rest of the measurements. This method may require additional analysis and for some routes, it may be difficult to determine which areas should be considered background. To estimate a temporally variable background over the course of a sampling run without specific designation of a background area, a 5–15 min minimum can be used (Fig. 7c). In this case, a rolling 11 s median was used to smooth the time series and then the minimum was calculated for each 5 min or 15 min discrete interval. A smooth curve was fit to the minima using a thin plate regression spline (Wood, 2003). Using a fixed temporal window relies on the assumption that the measurement platform will pass through an area of "clean" air within each interval. The route used for this analysis was so short that this

AMTD
6, 10443–10480, 2013

assumption is not a problem. However, this assumption may not be appropriate with longer routes that do not frequently encounter areas representative of background.

To calculate the temporal variation of the background without making assumptions about specific time intervals, a flexible window baseline algorithm was developed. This algorithm relies on the fact that background variation occurs over a larger time scale than spatial variation. The algorithm essentially looks for local minima along the time series, but restricts the baseline to change only gradually over time. The full algorithm description is available in Appendix A.

Background standardization will have the greatest effect on measurements of pollutants that have a high regional background concentration relative to the concentrations emitted by the source of interest. Of the mobile source pollutants measured in this study, $PM_{2.5}$, PM_{10}, NO_2, and CO_2 all fall into the category of co-emitted pollutants with high regional background concentrations ($\geq 50\,\%$ of the mean measured concentrations, Table 4). In contrast, CO, BC, and UFPs can all be classified as co-emitted pollutants with low regional background concentrations (Table 4). To compare the variation in background concentrations, the mean background value for each run was calculated and the between-run standard deviation (SD) was determined from the resulting 24 mean background values. Additionally, the within-run SD was calculated by first calculating the SD for each run and then taking the range of those values. The large differences in within-run SD are likely due to variations in the stability of meteorological conditions. For this reason, the range is given instead of the mean (Table 4). For CO and NO_2, the between-run SD was greater than all of the within-run SDs (Table 4), indicating that the daily variation of these pollutants was greater than the hourly variation. For the rest of the pollutants measured, the between-run SD fell within the range of the within-run SD. Kimbrough et al. (2013) also found that the background contribution of NO_2 to the total concentration was higher than the background contribution of CO and BC, with measured upwind concentrations approximately 69 %, 63 %, and 44 % of downwind concentrations for NO_2, CO, and BC, respectively. The background contributions measured by Kimbrough et al. (2013) are higher than those calculated

AMTD
6, 10443–10480, 2013

for the current study, likely because the downwind measurements were collected 20 m from the road, while many of the measurements in the current study were collected on the highway or on roads with high traffic volume causing the total concentrations to be higher and the fraction attributable to regional background to be lower. Upwind concentrations of UFPs measured by Hagler et al. (2009) were roughly 30 % of the nearest downwind site and about 50 % of the levels observed at 100 m from the road.

Before background standardization, the regional background variation obscured the spatial variation in $PM_{2.5}$ (Fig. 8a). Before background removal, $PM_{2.5}$ concentrations measured on Route B on a highway with an AADT of 109 000 were below the 50th percentile when compared with all of the measurements made over the course of the field campaign, while measurements collected on Route A on a road with an AADT of 18 000 and Route C on a road with an AADT of 17 000 were all above the 50th percentile (Fig. 8a). After the influence of the regional background was removed, the spatial trends become much more evident. The majority of the measurements collected on highways (AADT $\geq$ 100 000) fall in the higher percentiles, and measurements made on roads with less traffic fall in the lower percentiles of the dataset (Fig. 8b).

3.4 Temporal and spatial smoothing methods

The influence of temporal and spatial smoothing on the calculation of the concentration gradient along the highway transect analyzed in Sect. 4.2 was compared. The data shown were collected during two sampling runs conducted on 21 September 2012 and 11 October 2012 and were filtered using the running COV method. When compared to the raw data (Fig. 9a), spatial smoothing alone clarifies the trend (Fig. 9b). In contrast, although temporal smoothing results in fewer data points, the trend is still obscured (Fig. 9c). Furthermore, while spatial smoothing alone results in a fairly smooth gradient and the degree of spatial smoothing does not have a significant effect on the fitted curve (Fig. 9b), aggregating the data to a larger time scale before applying spatial smoothing introduces additional noise (Fig. 9d). This noise is due to the error introduced into the estimation of location by using a longer time scale. The slight increase

AMTD
6, 10443–10480, 2013

in concentrations at 500 m is due to a busy intersection at this location. The model $NO_2 = m \times \log(\text{distance}) + b$ was fit for each smoothing case because previous studies have found that pollutant concentrations tend to decrease exponentially with distance from a major source Karner et al. (2010).

Spatial and temporal smoothing also causes pollutant concentrations to become more correlated as measured by the Spearman correlation coefficients. The average speed of the car on this route was approximately 10 m s^{-1}. The Spearman correlation coefficients were calculated for BC, CO, CO_2, NO_2, $PM_{2.5}$ and UFPs after applying the COV filter and after calculating 5 s and 10 s averages (discrete windows) and dividing the route into 5 m, 50 m, and 100 m segments and calculating the average of the measurements in each segment. Spatial smoothing resulted in much stronger correlations compared to temporal smoothing (Table 5). NO_2 and CO_2 were slightly negatively correlated before smoothing. After temporal smoothing the correlation coefficient remained negative, but after spatial smoothing the correlation coefficient rose to 0.80. After 10 m averaging, all of the pollutants were correlated with coefficients greater than 0.7. After 50 m averaging all of the correlation coefficients were greater than 0.8, but increasing the averaging interval to 100 m did not change any coefficients by more than 0.02.

4 Conclusions

The recent increase in the number of studies that employ mobile monitoring and the variety of applications demonstrate both the utility and versatility of mobile monitoring. As air monitoring instumentation continues to advance toward greater portability, higher time resolution, greater capacity for operating autonomously, and lower costs, it is likely that these types of studies will become even more ubiquitous (Snyder et al., 2013). The greater temporal and geographic coverage of air pollution measurements can in turn lead to better protection of health and the environment. However, as was shown in this study, this new wealth of data requires the implementation of innovative data

AMTD
6, 10443–10480, 2013

proccessing techniques to extract meaningful information and develop intuitive visuals. This study investigated the sensitivity of final analysis results to the data processing steps chosen.

A variety of research questions and the corresponding data processing strategies were discussed, and a framework for deciding which strategies to apply was presented. Precise time alignment of instruments with each other and location data is particularly important for mobile platforms traveling at high speeds and emissions factor calculations. Removal of local emissions events can substantially change a near-source gradient, but the various methods of emissions event removal that were compared resulted in similar results. Background standardization was particularly important for pollutants with a high background concentration relative to the total concentration, and estimated background concentrations were shown to vary with time. Spatial averaging (50 m) resulted in smoother concentration gradients and stronger correlations than temporal averaging (5 s).

The results demonstrate the vast amount of information contained in datasets collected using mobile monitoring and the myriad of research questions that can be answered using these data, as well as the sensitivity of the conclusions to the data processing approach utilized.

Appendix A

Flexible window baseline algorithm

In this study, a new algorithm was developed to determine the background concentration as a function of time using a time series of concentrations (C_t) collected using a mobile monitoring vehicle, without using a fixed time interval. The algorithm consists of three phases: first, potential baseline points in the time series are identified, then the number of baseline points is thinned so that there is no more than one baseline point in each 5 min window, and finally a smooth function is fitted to the remaining baseline

AMTD
6, 10443–10480, 2013

points. Given a time series C_t that starts at t_0, the time of the first baseline point $t_{b,1}$ and the concentration of the first baseline point $C_{t_{b,1}}$ are determined by calculating the minimum of the first 15 min of data so that

$$(C_{t_{b,1}}) = \text{minimum}(C_t)$$
$$\text{where}: \; t = [t_0, t_0 + 15\,\text{min}] \tag{A1}$$

Then a 15 min window $[t_{b,1}, t_{b,1} + 15\,\text{min}]$ is used to locate the next baseline point ($t_{b,2}$), which (if available) is the first occurrence where $C_t \le C_{t_{b,1}}$. If $C_t > C_{t_{b,1}}$ for all $t = [t_{b,1}, t_{b,1} + 15\,\text{min}]$, then $t_{b,2}$ is the first occurrence where:

$$C_t \le C_{t_{b,1}} + \theta$$
$$\text{where: } t = [t_{b,1}, t_{b,1} + 15\,\text{min}] \tag{A2}$$

with the threshold, θ, equal to the twice the standard deviation of the lowest 10 % of the measured concentrations. The 15 min window is then shifted to $[t_{b,2}, t_{b,2} + 15\,\text{min}]$ and the algorithm repeats. If $C_t > C_{t_{b,1}} + \theta$ for all $t = [t_{b,1}, t_{b,1} + 15\,\text{min}]$, then it is assumed that the mobile platform did not pass through an area of background in that window and the window is shifted forward another 15 min so that $t = [t_{b,1} + 15\,\text{min}, t_{b,1} + 30\,\text{min}]$ and the algorithm repeats. At the completion of this first pass, extraneous baseline points are removed by taking the minimum of the baseline points in each 5 min discrete window. A smooth thin plate regression spline is fitted to the remaining points (Fig. A1).

Acknowledgements. This research would not have been possible without the careful field measurements conducted by ARCADIS employee Parikshit Deshmukh under contract EP-C-09-027. The authors are also grateful for the research support provided by a number of EPA staff in the Office of Research and Development, particulary Richard Shores, Bill Mitchell, and Robert Wright.

AMTD
6, 10443–10480, 2013

Disclaimer. This document has been reviewed in accordance with the US Environmental Protection Agency policy and approved for publication. Mention of trade names or commercial products does not constitute endorsement or recommendation for use. The views expressed in this journal article are those of the authors and do not necessarily reflect the views or policies or the US Environmental Protection Agency.

References

Adams, M. D., DeLuca, P. F., Corr, D., and Kanaroglou, P. S.: Mobile air monitoring: measuring change in air quality in the city of Hamilton, 2005–2010, Soc. Indic. Res., 108, 351–364, 2012. 10445, 10466

Arku, R. E., Vallarino, J., Dionisio, K. L., Willis, R., Choi, H., Wilson, J. G., Hemphill, C., Agyei-Mensah, S., Spengler, J. D., and Ezzati, M.: Characterizing air pollution in two low-income neighborhoods in Accra, Ghana, Sci. Total. Environ., 402, 217–231, 2008. 10445, 10452, 10466, 10467

Baldauf, R., Thoma, E., Khlystov, A., Isakov, V., Bowker, G., Long, T., and Snow, R.: Impacts of noise barriers on near-road air quality, Atmos. Environ., 42, 7502–7507, 2008. 10445

Bukowiecki, N., Dommen, J., Prevot, A., Richter, R., Weingartner, E., and Baltensperger, U.: A mobile pollutant measurement laboratory – measuring gas phase and aerosol ambient concentrations with high spatial and temporal resolution, Atmos. Environ., 36, 5569–5579, 2002. 10452, 10455, 10467

Carslaw, D. C. and Ropkins, K.: Openair – an R package for air quality data analysis, Environ. Modell. Softw., 27–28, 52–61, 2012. 10449

Choi, W., He, M., Barbesant, V., Kozawa, K. H., Mara, S., Winer, A. M., and Paulson, S. E.: Prevalence of wide area impacts downwind of freeways under pre-sunrise stable atmospheric conditions, Atmos. Environ., 62, 318–327, 2012. 10445, 10449, 10450, 10451, 10454, 10466, 10467

Dionisio, K. L., Rooney, M. S., Arku, R. E., Friedman, A. B., Hughes, A. F., Vallarino, J., Agyei-Mensah, S., Spengler, J. D., and Ezzati, M.: Within-neighborhood patterns and sources of particle pollution: mobile monitoring and geographic information system analysis in four communities in Accra, Ghana, Environ. Health Perspect., 118, 607–613, 2010. 10466, 10467

AMTD
6, 10443–10480, 2013

Drewnick, F., Böttger, T., von der Weiden-Reinmüller, S.-L., Zorn, S. R., Klimach, T., Schneider, J., and Borrmann, S.: Design of a mobile aerosol research laboratory and data processing tools for effective stationary and mobile field measurements, Atmos. Meas. Tech., 5, 1443–1457, doi:10.5194/amt-5-1443-2012, 2012. 10445, 10450, 10454, 10467

Durant, J. L., Ash, C. A., Wood, E. C., Herndon, S. C., Jayne, J. T., Knighton, W. B., Canagaratna, M. R., Trull, J. B., Brugge, D., Zamore, W., and Kolb, C. E.: Short-term variation in near-highway air pollutant gradients on a winter morning, Atmos. Chem. Phys., 10, 8341–8352, doi:10.5194/acp-10-8341-2010, 2010. 10445

ESRI: ArcGIS Desktop: Release 10, Environmental Systems Research Institute, Redlands, CA, USA, 2011. 10449

Farrell, P., Culling, D., and Leifer, I.: Transcontinental methane measurements: Part 1. A mobile surface platform for source investigations, Atmos. Environ., 74, 422–431, 2013. 10445

Hagler, G., Baldauf, R., Thoma, E., Long, T., Snow, R., Kinsey, J., Oudejans, L., and Gullett, B.: Ultrafine particles near a major roadway in Raleigh, North Carolina: downwind attenuation and correlation with traffic-related pollutants, Atmos. Environ., 43, 1229–1234, 2009. 10457

Hagler, G. S. W., Thoma, E. D., and Baldauf, R. W.: High-resolution mobile monitoring of carbon monoxide and ultrafine particle concentrations in a near-road environment, J. Air Waste Manag. Assoc., 60, 328–336, 2010. 10445, 10448

Hagler, G., Yelverton, T., Vedantham, R., Hansen, A., and Turner, J.: Post-processing method to reduce noise while preserving high time resolution in aethalometer real-time black carbon data, Aerosol Air Qual. Res., 11, 539–546, 2011. 10449

Hagler, G. S. W., Lin, M.-Y., Khlystov, A., Baldauf, R. W., Isakov, V., Faircloth, J., and Jackson, L. E.: Field investigation of roadside vegetative and structural barrier impact on near-road ultrafine particle concentrations under a variety of wind conditions, Sci. Total. Environ., 419, 7–15, 2012. 10445, 10450, 10451, 10452, 10454, 10455, 10466, 10467, 10475

Hu, S., Paulson, S. E., Fruin, S., Kozawa, K., Mara, S., and Winer, A. M.: Observation of elevated air pollutant concentrations in a residential neighborhood of Los Angeles California using a mobile platform, Atmos. Environ., 51, 311–319, 2012. 10445, 10466

Karner, A. A., Eisinger, D. S., and Niemeier, D. A.: Near-roadway air quality: synthesizing the findings from real-world data, Environ. Sci. Technol., 44, 5334–5344, 2010. 10454, 10458

Kimbrough, S., Baldauf, R. W., Hagler, G. S., Shores, R. C., Mitchell, W., Whitaker, D. A., Croghan, C. W., and Vallero, D. A.: Long-term continuous measurement of near-road air

AMTD
6, 10443–10480, 2013

pollution in Las Vegas: seasonal variability in traffic emissions impact on local air quality, Air Qual. Atmos. Health, 6, 295–305, 2013. 10456

Kolb, C. E., Herndon, S. C., McManus, J. B., Shorter, J. H., Zahniser, M. S., Nelson, D. D., Jayne, J. T., Canagaratna, M. R., and Worsnop, D. R.: Mobile laboratory with rapid response instruments for real-time measurements of urban and regional trace gas and particulate distributions and emission source characteristics, Environ. Sci. Technol., 38, 5694–5703, 2004. 10467

Kozawa, K. H., Fruin, S. A., and Winer, A. M.: Near-road air pollution impacts of goods movement in communities adjacent to the Ports of Los Angeles and Long Beach, Atmos. Environ., 43, 2960–2970, 2009. 10445, 10466, 10467

Ligges, U. and Mächler, M.: Scatterplot3d – an R Package for Visualizing Multivariate Data, J. Stat. Softw., 8, 1–20, 2003. 10449

Massoli, P., Fortner, E. C., Canagaratna, M. R., Williams, L. R., Zhang, Q., Sun, Y., Schwab, J. J., Trimborn, A., Onasch, T. B., Demerjian, K. L., Kolb, C. E., Worsnop, D. R., and Jayne, J. T.: Pollution gradients and chemical characterization of particulate matter from vehicular traffic near major roadways: results from the 2009 Queens College Air Quality study in NYC, Aerosol Sci. Tech., 46, 1201–1218, 2012. 10445

MATLAB: version 7.14.0 (R2010a), The MathWorks Inc., Natick, Massachusetts, 2012. 10449

Padró-Martínez, L. T., Patton, A. P., Trull, J. B., Zamore, W., Brugge, D., and Durant, J. L.: Mobile monitoring of particle number concentration and other traffic-related air pollutants in a near-highway neighborhood over the course of a year, Atmos. Environ., 61, 253–264, 2012. 10466

Park, S. S., Kozawa, K., Fruin, S., Mara, S., Hsu, Y.-K., Jakober, C., Winer, A., and Herner, J.: Emission factors for high-emitting vehicles based on on-road measurements of individual vehicle exhaust with a mobile measurement platform, J. Air Waste Manag. Assoc., 61, 1046–1056, 2011. 10445, 10449, 10450, 10466

Pirjola, L., Lähde, T., Niemi, J., Kousa, A., Rönkkö, T., Karjalainen, P., Keskinen, J., Frey, A., and Hillamo, R.: Spatial and temporal characterization of traffic emissions in urban microenvironments with a mobile laboratory, Atmos. Environ., 63, 156–167, 2012. 10447

Pétron, G., Frost, G., Miller, B. R., Hirsch, A. I., Montzka, S. A., Karion, A., Trainer, M., Sweeney, C., Andrews, A. E., and Miller, L.: Hydrocarbon emissions characterization in the Colorado Front Range: A pilot study, J. Geophys. Res.-Atmos., 117, D04304, doi:10.1029/2011JD016360, 2012. 10466

AMTD
6, 10443–10480, 2013

R Core Team: R: A Language and Environment for Statistical Computing, R Foundation for Statistical Computing, Vienna, Austria, available at: http://www.R-project.org/ (last access: 22 June 2012), ISBN 3-900051-07-0, 2012. 10449

Rooney, M. S., Arku, R. E., Dionisio, K. L., Paciorek, C., Friedman, A. B., Carmichael, H., Zhou, Z., Hughes, A. F., Vallarino, J., and Agyei-Mensah, S.: Spatial and temporal patterns of particulate matter sources and pollution in four communities in Accra, Ghana, Sci. Total. Environ., 435, 107–114, 2012. 10445

Snyder, E. G., Watkins, T., Solomon, P., Thoma, E., Williams, R., Hagler, G., Shelow, D., Hindin, D., Kilaru, V., and Preuss, P.: The changing paradigm of air pollution monitoring, Environ. Sci. Technol., 47, 11369–11377, 2013. 10458

Van Poppel, M., Peters, J., and Bleux, N.: Methodology for setup and data processing of mobile air quality measurements to assess the spatial variability of concentrations in urban environments, Environ. Pollut., 183, 224–233, 2013. 10445, 10447, 10452, 10455, 10466, 10467

Wallace, J., Corr, D., Deluca, P., Kanaroglou, P., and McCarry, B.: Mobile monitoring of air pollution in cities: the case of Hamilton, Ontario, Canada, J. Environ. Monitor., 11, 998–1003, 2009. 10466

Wang, X., Westerdahl, D., Chen, L. C., Wu, Y., Hao, J., Pan, X., Guo, X., and Zhang, K. M.: Evaluating the air quality impacts of the 2008 Beijing Olympic Games: on-road emission factors and black carbon profiles, Atmos. Environ., 43, 4535–4543, 2009. 10445, 10466

Wang, X., Westerdahl, D., Wu, Y., Pan, X., and Zhang, K. M.: On-road emission factor distributions of individual diesel vehicles in and around Beijing, China, Atmos. Environ., 45, 503–513, 2011. 10445

Wang, X., Westerdahl, D., Hu, J., Wu, Y., Yin, H., Pan, X., and Max Zhang, K.: On-road diesel vehicle emission factors for nitrogen oxides and black carbon in two Chinese cities, Atmos. Environ., 46, 45–55, 2012. 10445

Weijers, E., Khlystov, A., Kos, G., and Erisman, J.: Variability of particulate matter concentrations along roads and motorways determined by a moving measurement unit, Atmos. Environ., 38, 2993–3002, 2004. 10447

Westerdahl, D., Fruin, S., Sax, T., Fine, P. M., and Sioutas, C.: Mobile platform measurements of ultrafine particles and associated pollutant concentrations on freeways and residential streets in Los Angeles, Atmos. Environ., 39, 3597–3610, 2005. 10445, 10447

AMTD
6, 10443–10480, 2013

Westerdahl, D., Wang, X., Pan, X., and Zhang, K. M.: Characterization of on-road vehicle emission factors and microenvironmental air quality in Beijing, China, Atmos. Environ., 43, 697–705, 2009. 10445

Wood, S. N.: Thin-plate regression splines, J. Roy. Stat. Soc. B, 65, 95–114, 2003. 10449, 10455

Zwack, L. M., Paciorek, C. J., Spengler, J. D., and Levy, J. I.: Characterizing local traffic contributions to particulate air pollution in street canyons using mobile monitoring techniques, Atmos. Environ., 45, 2507–2514, 2011a. 10445, 10452, 10466, 10467

Zwack, L. M., Paciorek, C. J., Spengler, J. D., and Levy, J. I.: Modeling spatial patterns of traffic-related air pollutants in complex urban terrain, Environ. Health Persp., 119, 852–859, 2011b. 10452, 10466, 10467

AMTD
6, 10443–10480, 2013

Table 1. Mobile monitoring example applications.

Category	Example Investigations	Measurement Platform	Data Processing Steps Applied	References
Emissions Quantification	Determine and compare emissions factors from vehicles under various driving conditions	Electric vehicle	Emissions event detection, temporal smoothing	Park et al. (2011)
	Evaluate change in emissions factors after traffic intervention	Vehicle	Emissions event detection, background standardization, temporal smoothing	Wang et al. (2009)
	Hydrocarbon emissions characterization	Vehicle	Emissions event detection	Pétron et al. (2012)
Near-source air quality gradients and mitigation strategy evaluation	Roadside barrier impacts	Electric vehicle	Emissions event detection, background standardization, spatial smoothing	Hagler et al. (2012)
	Near-road gradients	Electric vehicle	Time alignment optimization, emissions event detection, background standardization, spatial smoothing	Kozawa et al. (2009); Choi et al. (2012)
	Assess contribution of traffic in street canyons to concentration above background	Backpack	Background standardization, spatial smoothing	Zwack et al. (2011a, b)
	Characterize spatial and temporal variation of near-road gradients	Recreational Vehicle	Temporal and spatial smoothing	Padró-Martínez et al. (2012)
General air quality surveying	Change in air quality in City of Hamilton, 2005–2010	Van	Background standardization, temporal smoothing	Adams et al. (2012); Wallace et al. (2009)
	Characterizing pollution in low-income neighborhoods in Ghana	Handheld	Background standardization, spatial smoothing	Arku et al. (2008); Dionisio et al. (2010)
	Spatial variability of urban air quality	Bicycle	Background standardization, spatial smoothing	Van Poppel et al. (2013)
	Characterize exposure zones	Electric vehicle	Emissions event detection	Hu et al. (2012)

AMTD
6, 10443–10480, 2013

Table 2. Mobile data processing methods.

Category	Method Description	References
Background Estimation	Designation of background zone	Hagler et al. (2012); Van Poppel et al. (2013)
	Average of fixed monitoring sites	Arku et al. (2008); Dionisio et al. (2010)
	1 min or 5 min 5th percentile	Bukowiecki et al. (2002)
	Assume all of the measurements lower than the most frequent measurement are background	Kolb et al. (2004)
	Include a smooth function of time over each sampling shift as a term in a linear regression	Zwack et al. (2011b, a)
Emissions Event Detection	Calculate standard deviation of measurements below the median (σ_b). Flag any measurement more than $3\sigma_b$ greater than the previous measurement. Flag all measurements $> 3\sigma_b + \sqrt{n} \times \sigma_b$ from the last non-flagged measurement, where n is the number of points since the last non-flagged measurement (UFPs[a] and CO_2[b])	Drewnick et al. (2012)
	Modified 5 s running coefficient of variance, with maximum value of 2 (UFP[a])	Hagler et al. (2012)
	Smoothed rolling minimum (CO_2[b], NO[c])	Kolb et al. (2004)
	Rolling 25th percentile (UFPs[a], NO[c], PB–PAH[d], CO[f], $PM_{2.5}$[g])	Choi et al. (2012)
	Video records were checked at times when pollution concentrations peaked at greater than twice the observed background concentrations (BC[e], NO[c], UFP[a], PB–PAH[d])	Kozawa et al. (2009)

[a]Ultrafine particles (≤ 100 nm), [b]carbon dioxide, [c]nitrogen monoxide, [d]particle-bound polycyclic aromatic hydrocarbon, [e]black carbon, [f]carbon monoxide, [g]particulate matter (≤ 2.5 µm).

AMTD
6, 10443–10480, 2013

Table 3. Emissions factors before and after temporal alignment using cross-correlation.

	BC ($g\,kg^{-1}$)	UFP ($\#\,kg^{-1}$)	CO ($g\,kg^{-1}$)
No alignment adjustment (1 s)	0.024	2.17×10^{15}	0.016
With alignment adjustment (1 s)	0.032	2.16×10^{15}	0.015
No alignment adjustment, temporal smoothing (10 s)	0.066	3.07×10^{15}	0.019
With alignment adjustment and temporal smoothing (10 s)	0.042	2.43×10^{15}	0.017

AMTD
6, 10443–10480, 2013

Table 4. Summary comparison of pollutant background concentration and variation.

	Mean of Background	Within Run SD[a,b]	Between Run SD[c]	Contribution of Background to Total[d]
BC ($\mu g\,m^{-3}$)	0.19	0.01–0.48	0.16	6 %
$PM_{2.5-10}$ ($\mu g\,m^{-3}$)	0.5	0.0–0.7	0.51	12 %
UFP (cm^{-3})	3800	20–2150	1600	19 %
CO (ppb)	278	1–38	74	38 %
PM_{10} ($\mu g\,m^{-3}$)	4.5	0.0–2.9	1.9	45 %
NO_2 (ppb)	8.0	0.2–2.2	2.4	51 %
$PM_{2.5}$ ($\mu g\,m^{-3}$)	3.1	0.1–2.1	1.5	56 %
CO_2 (ppm)	435	1–69	37	86 %

[a]Standard deviation, [b]calculated by first calculating the SD of the estimated background for each run and then taking the range of those values, [c]calculated by determining the mean background value for each run and determining the standard deviation of the resulting 24 mean background values, [d]mean of estimated background for all 24 runs divided by mean measured concentration of all runs multiplied by 100.

AMTD
6, 10443–10480, 2013

Table 5. Effect of temporal and spatial smoothing on pollutant Spearman correlation coefficients.

	Filtered Raw Data	Temporal Smoothing 5 s	Temporal Smoothing 10 s	Spatial Smoothing 10 m	Spatial Smoothing 50 m	Spatial Smoothing 100 m
	$N = 8386$	$N = 1801$	$N = 921$	$N = 529$	$N = 105$	$N = 52$
NO_2 (ppb) and CO_2 (ppm)	−0.21	−0.19	−0.19	0.71	0.80	0.80
NO_2 (ppb) and $PM_{2.5}$ ($\mu g\,m^{-3}$)	0.07	0.10	0.12	0.77	0.85	0.86
NO_2 (ppb) and BC ($\mu g\,m^{-3}$)	0.11	0.12	0.12	0.76	0.81	0.80
CO (ppb) and NO_2 (ppb)	0.16	0.18	0.18	0.81	0.85	0.85
UFP (cm^{-3}) and CO_2 (ppm)	0.36	0.39	0.40	0.82	0.90	0.91
UFP (cm^{-3}) and $PM_{2.5}$ ($\mu g\,m^{-3}$)	0.41	0.53	0.57	0.83	0.89	0.89
UFP (cm^{-3}) and BC ($\mu g\,m^{-3}$)	0.47	0.53	0.58	0.80	0.85	0.86
BC ($\mu g\,m^{-3}$) and $PM_{2.5}$ ($\mu g\,m^{-3}$)	0.54	0.69	0.74	0.77	0.82	0.84
NO_2 (ppb) and UFP (cm^{-3})	0.56	0.60	0.62	0.88	0.87	0.87
CO (ppb) and UFP (cm^{-3})	0.58	0.63	0.65	0.88	0.92	0.92
$PM_{2.5}$ ($\mu g\,m^{-3}$) and CO_2 (ppm)	0.60	0.72	0.75	0.80	0.84	0.86
CO (ppb) and $PM_{2.5}$ ($\mu g\,m^{-3}$)	0.61	0.73	0.76	0.84	0.86	0.86
BC ($\mu g\,m^{-3}$) and CO_2 (ppm)	0.68	0.73	0.76	0.82	0.87	0.88
CO (ppb) and BC ($\mu g\,m^{-3}$)	0.69	0.74	0.76	0.81	0.85	0.87
CO (ppb) and CO_2 (ppm)	0.78	0.78	0.79	0.87	0.92	0.92

AMTD
6, 10443–10480, 2013

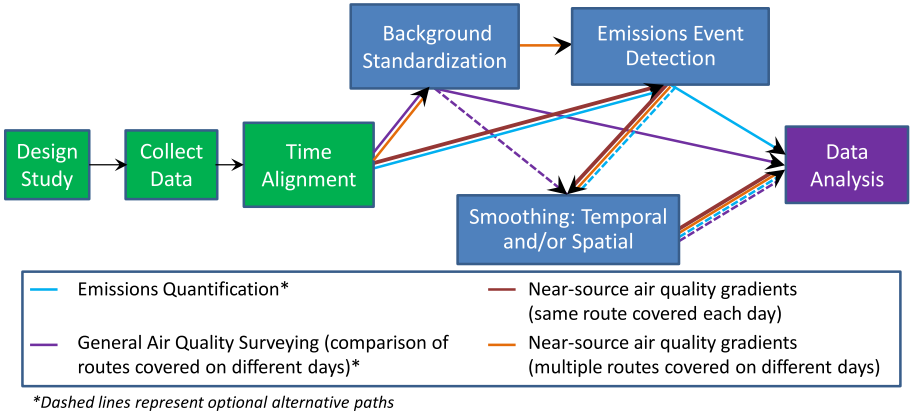

Fig. 1. Mobile data processing steps.

AMTD
6, 10443–10480, 2013

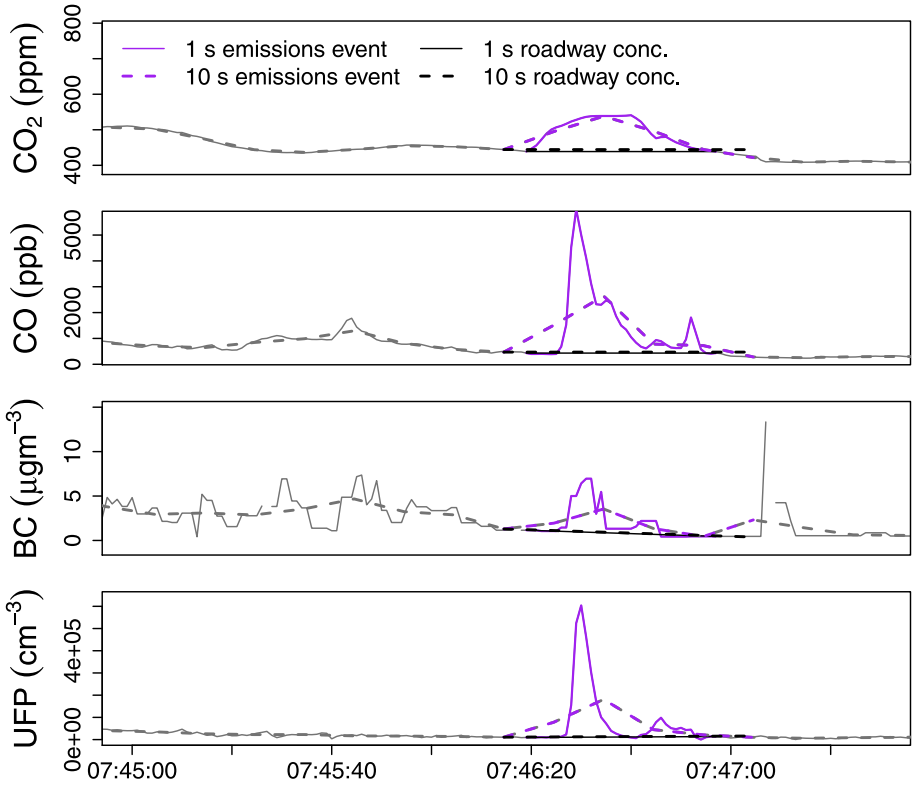

Fig. 2. Emissions factor calculation using peak from local emissions event. Dashed lines represent 10 s averages. Purple lines represent emissions event. Black lines represent roadway concentrations.

AMTD
6, 10443–10480, 2013

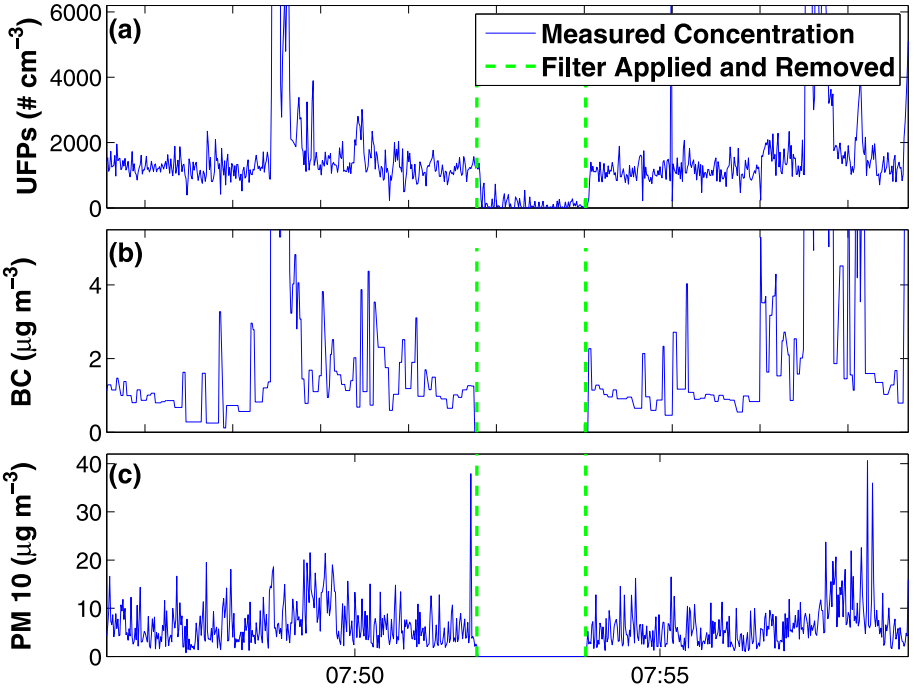

Fig. 3. Quality control check on PM instruments: UFPs **(a)**, BC **(b)**, and PM_{10} **(c)**.

AMTD
6, 10443–10480, 2013

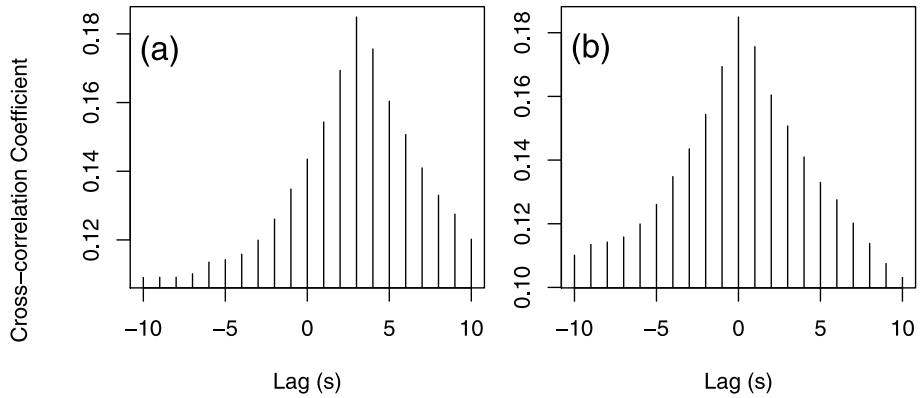

Fig. 4. Cross correlation between CO and BC before lag time adjustment **(a)** and after lag time adjustment **(b)**.

AMTD
6, 10443–10480, 2013

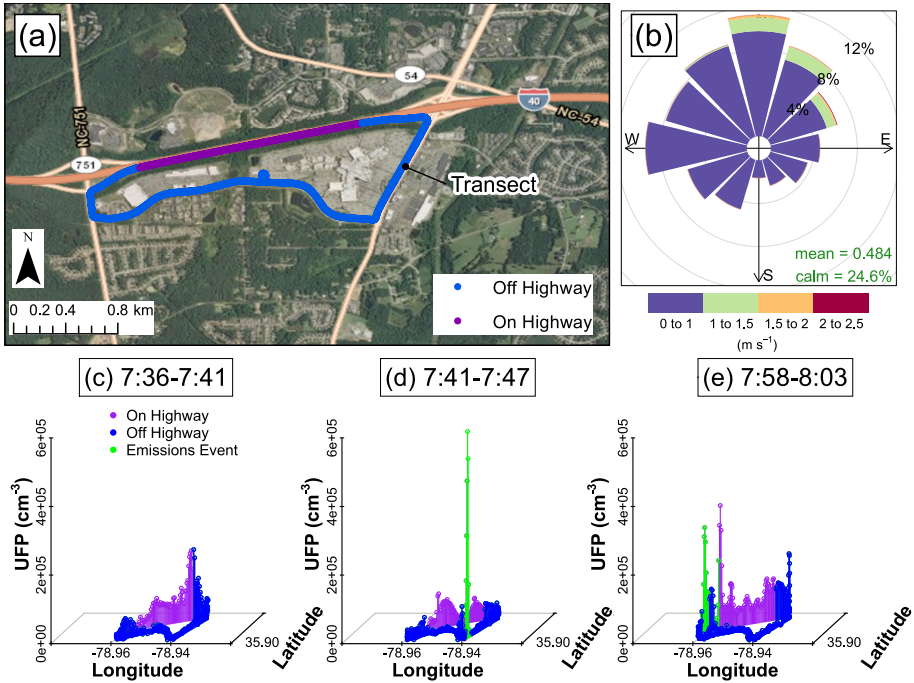

Fig. 5. Map of route **(a)** wind rose **(b)** and measured UFP concentration (cm^{-3}) on three laps **(c–e)**. Green lines represent emissions events identified using the modified COV filter (Hagler et al., 2012).

AMTD
6, 10443–10480, 2013

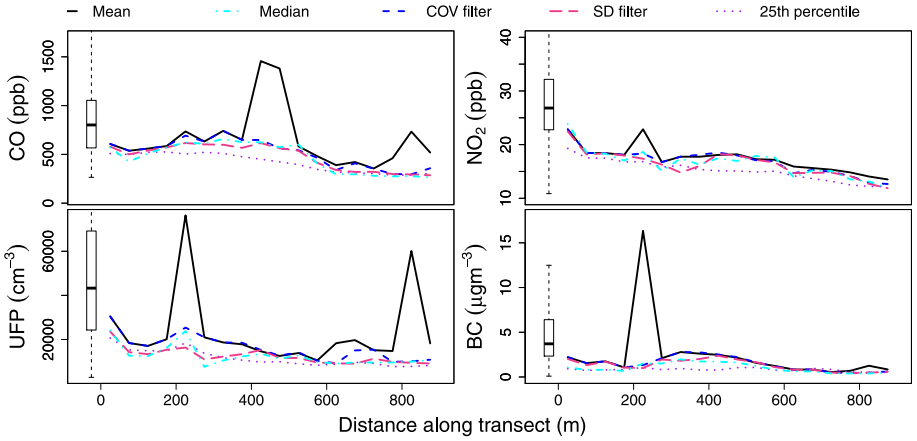

Fig. 6. Comparison of filtering methods on transect gradients of CO **(a)**, UFP **(b)**, BC **(c)**, and NO_2 **(d)**. Lines represent 50 m averages of measurements from the entire run (9 laps). Boxplots represent unfiltered concentrations measured on the highway.

AMTD
6, 10443–10480, 2013

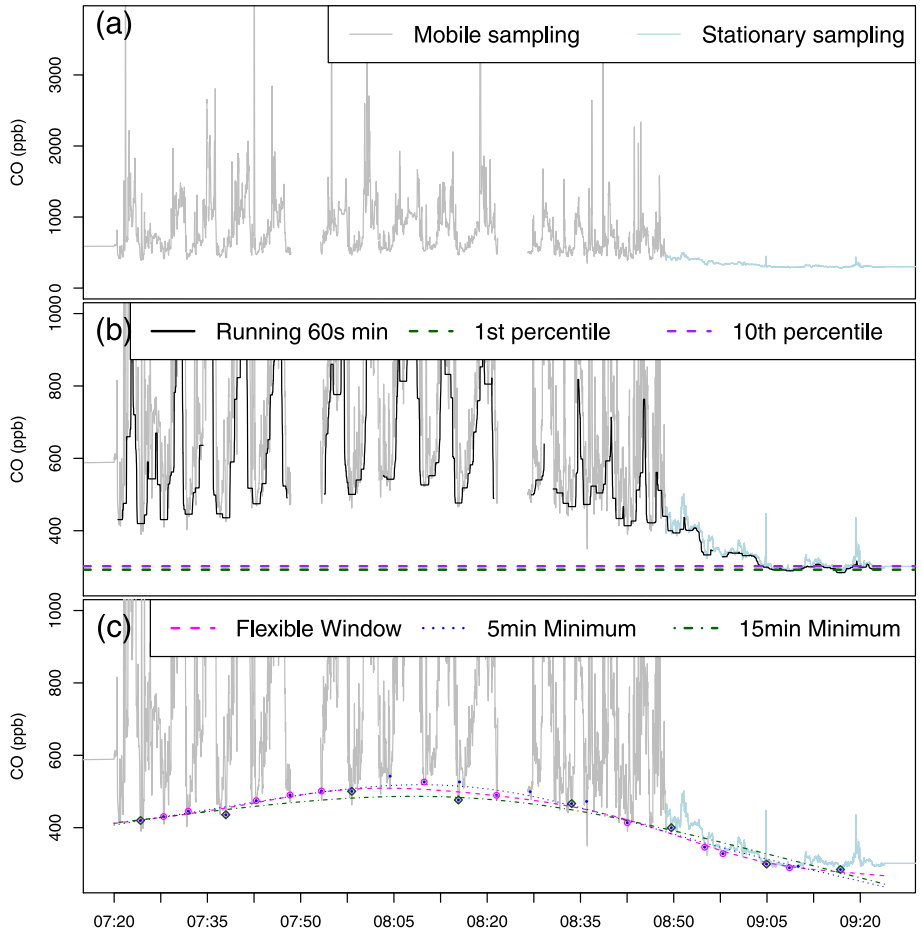

Fig. 7. Background removal methods and new algorithm for time varying background: **(a)** example time series; **(b)** running minimum, 1st percentile and 10th percentile; **(c)** flexible window algorithm, 5 min minimum, and 15 min minimum.

AMTD
6, 10443–10480, 2013

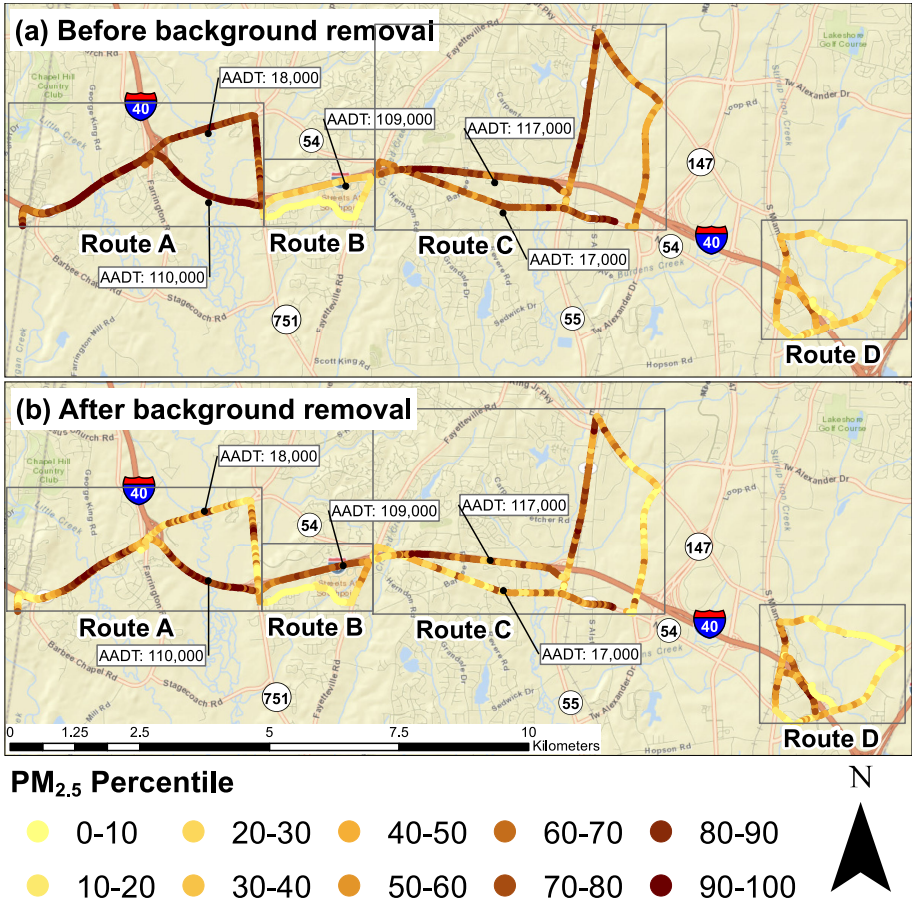

Fig. 8. Spatial distribution of $PM_{2.5}$ before **(a)** and after **(b)** background standardization. Points represent median 50 m values from 8 sampling runs with each route measured on 2 days.

AMTD
6, 10443–10480, 2013

Mobile air monitoring data processing strategies and effects

H. L. Brantley et al.

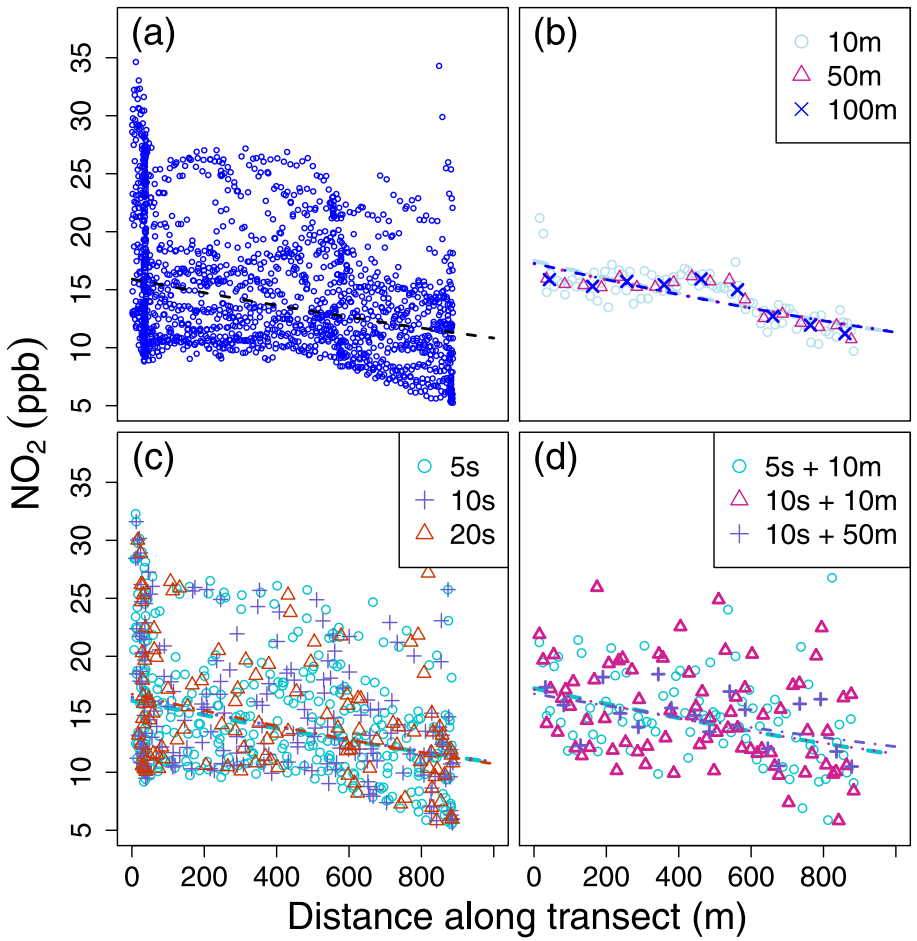

Fig. 9. Comparison of temporal and spatial smoothing.

AMTD
6, 10443–10480, 2013

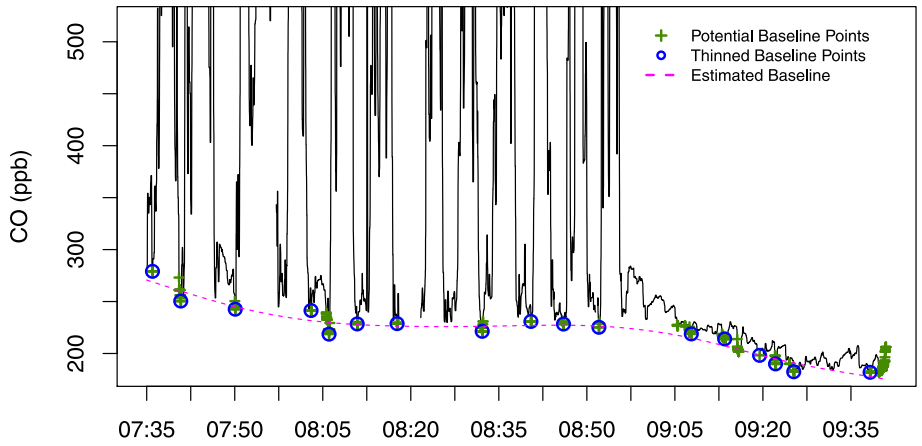

Fig. A1. Illustration of baseline algorithm.

AMTD
6, 10443–10480, 2013